# Half-life of $^{228}$Pu and $\alpha$ decay of $^{228}$Np

K. Nishio,[1] H. Ikezoe,[1] S. Mitsuoka,[1] K. Satou,[1] and C. J. Lin[1,2]
[1]*Advanced Science Research Center, Japan Atomic Energy Research Institute, Tokai, Ibaraki 319-1195, Japan*
[2]*China Institute of Atomic Energy, Beijing 102413, China*
(Received 17 April 2003; published 11 December 2003)

Two $\alpha$-decay chains starting from $^{228}$Pu produced in the reaction of $^{34}$S+$^{198}$Pt were observed, and the half-life was measured to be $1.1^{+2.0}_{-0.5}$ s. The half-life follows the Geiger-Nuttall curve for even-even Pu isotopes, which shows that $\alpha$ decay is the dominant decay mode. In addition, five $\alpha$-decay events of $^{228}$Np were observed for the first time. The evaporation residue cross sections of $^{228}$Pu, $^{228}$Np, and $^{225}$U are reproduced by a statistical model calculation.

DOI: 10.1103/PhysRevC.68.064305 PACS number(s): 21.10.Tg, 23.60.+e, 27.90.+b, 25.70.Jj

## I. INTRODUCTION

Plutonium-228 was produced and identified for the first time by Andreyev *et al.* [1] in the fusion reaction of $^{24}$Mg +$^{208}$Pb. However, they were not able to determine the half-life of $^{228}$Pu.

In the present paper we report on the first measurement of half-life of $^{228}$Pu produced in the fusion reaction $^{34}$S+$^{198}$Pt (compound nucleus $^{232}$Pu). Our experimental method is similar to that in Ref. [1]. The evaporation residues (ERs) were separated by the JAERI recoil mass separator (JAERI-RMS) [2], and then implanted into a focal plane detector. The identification of the nucleus was made by observing the $\alpha$-decay chain. The lifetime of the ER is measured by the time interval between the recoil implantation and its $\alpha$ decay. In-flight separation allows us to measure the nucleus with a short half-life.

For the actinide nuclei with proton number of $Z$=90–94 and neutron number of $N$=134–138, $\alpha$-particle emission and electron capture (EC) are two competing decay modes. For $^{228}$Pu, a calculation suggests that the $\alpha$-decay partial half-life, $T_{\alpha,1/2}$=0.42 s [3], is two orders of magnitude shorter than that of EC decay $T_{\mathrm{EC},1/2}$=44 s [4]. It is known that the Geiger-Nuttall curve shows the relation between the partial half-life $T_{\alpha,1/2}$ and $Q$ value $Q_\alpha$ of $\alpha$ decay. If the experimental half-life follows this curve, one can estimate that the decay is dominated by $\alpha$ decay.

In addition, the $\alpha$ decay of $^{228}$Np was observed in the present measurement. The first production of this nucleus was made by Kuznetsov *et al.* [5], who determined the half-life of fission activity as 60 s in the reaction $^{22}$Ne+$^{209}$Bi. The EC-delayed fission properties of $^{228}$Np was studied by Kreek *et al.* [6] in detail. So far there is no report on the measurement of the $\alpha$ decay of $^{228}$Np.

The ER cross sections for $^{228}$Pu, $^{228}$Np, and $^{225}$U were also determined. The results were compared with a statistical model calculation, and the discussions are given in this paper.

## II. EXPERIMENT

The fusion reaction $^{34}$S+$^{198}$Pt was used to produce the neutron deficient nuclei $^{228}$Pu($4n$), $^{228}$Np($p3n$), and $^{225}$U($\alpha 3n$). The $^{34}$S ions were accelerated to $E_{\mathrm{beam}}$=170 and 172 MeV by the JAERI-tandem accelerator and irradiated a $^{198}$Pt target. Typical beam current was 40–50 pnA. The target with thickness 390 $\mu$g/cm$^2$ was made by sputtering an enriched $^{198}$Pt material (98%) on a 1.2-$\mu$m- thick aluminum (Al) foil. The above bombarding energy corresponds to the center-of-mass energy ($E_{\mathrm{c.m.}}$) of 141 and 143 MeV, respectively, at the half depth of the target layer, which was determined by calculating the energy loss of the beam in the Al foil and target.

The evaporation residues emitted in the beam direction were separated in flight from the primary beams and other reaction products by the JAERI-RMS. Before entering the recoil mass separator, the ER's charge state was reset by passing through a 30 $\mu$g/cm$^2$ carbon foil (charge reset foil). The detection efficiencies of ERs by the JAERI-RMS were calculated by the method described in Ref. [7], where we obtained good agreement between the measured detection efficiency and that calculated by using a program code GIOS [8]. The angular distributions of ERs were estimated by using the statistical model code PACE2 [9]. The multiple scattering of the ERs in the target and the charge reset foil were estimated by the TRIM code [10]. The JAERI-RMS was set to transport particles of $16^+$ charge state, which has the probability of 0.18 [11] in the charge state distribution. This probability was multiplied by the transport efficiency through the JAERI-RMS to yield the detection efficiency. Thus, the detection efficiencies for $4n$, $p3n$, and $\alpha 3n$ channels are determined to be 0.086, 0.074, and 0.050, respectively. The same procedure was also adopted in the previous measurement of ER cross sections [12].

The ERs transported through the JAERI-RMS were implanted into a double-sided position-sensitive silicon detector (PSD; $73\times55$ mm$^2$) located in the focal plane. The identification of the nucleus is made by constructing an $\alpha$-decay chain and finding the known $\alpha$-particle energies (and also lifetimes) of descendants, whose decay position agrees with that of the recoil implantation. The front side of PSD contains 15 position-sensitive strips with resistive layer. The signals induced on both sides of each strip were amplified with a shaping time of 0.3 $\mu$s, and the pulse heights give the energy and position of $X$. The backside is divided into eight sections, and the position $Y$ in each section can be deter-

 

mined. The pulse heights were digitized by an analog-to-digital converter with the gate width of 1 $\mu$s.

The $\alpha$ decay in the PSD is distinguished from the transported particle by determining that no time-of-flight (TOF) signal is present, which is measured by two timing detectors separated by the distance of 30 cm and placed upstream the PSD. In the off-line data analysis, the ERs were separated from the scattered beam particles on the two-dimensional spectrum of the TOF versus energy. This process considerably reduces the chance coincidence in finding a *recoil*-$\alpha$ correlation. Here, *recoil* means the event of the ER to hit the PSD. The dead time arising from the data acquisition process is 200 $\mu$s, and an $\alpha$ decay whose lifetime is shorter than the period will be missed.

The energy calibration of the PSD was made using $\alpha$ lines from the known nuclei [13], $^{216}$Th($E_\alpha$=7921 keV), $^{212}$Ra(6899), $^{215}$Ac(7604), $^{211}$Fr(6534), $^{211}$Ra(6910), $^{207}$Rn(6131), $^{215}$Th(7524, 7395), $^{210}$Ra(7019), and $^{206}$Rn(6258), produced in the reaction $^{34}$S+$^{186}$W. In this measurement, we constructed the spectra of position difference ($\Delta X$ and $\Delta Y$) between the recoil implantation and $\alpha$ decay for the chains of *recoil*-$\alpha$($^{216}$Th)-$\alpha$($^{212}$Ra) and *recoil*-$\alpha$($^{215}$Th)-$\alpha$($^{211}$Ra). The widths of $\Delta X$ and $\Delta Y$ spectra were 0.15 mm and 0.26 mm [full width at half maximum (FWHM)], respectively. In the data analysis we searched for the correlated $\alpha$-decay event whose position agreement is ($|\Delta X|$,$|\Delta Y|$) $<$(0.2, 0.4) mm.

The gain stability of the detection system was checked by exposing the PSD to $\alpha$ particles from an $^{241}$Am source. Typical energy resolution of the PSD was 75 keV (FWHM). In the data analysis, the discrimination level was set at about 2 MeV.

### III. EXPERIMENTAL RESULTS AND DISCUSSIONS

Figure 1 shows the energy spectrum obtained from the PSD. The spectrum (a) shows the events which do not generate TOF signals and includes all events taken during a 41-h run at the reaction energy of $E_{\mathrm{c.m.}}$=141 MeV. The large peak at 5.4 MeV represents $\alpha$ particles from the external $\alpha$ source ($^{241}$Am) which irradiated the silicon detector during the measurement. The broad 2–6 MeV spectrum is formed by scattered beam particles transported through the JAERI-RMS. As the detection efficiency of the timing detectors was not 100%, such background particles are not fully rejected and appear in the spectrum (a). There are several $\alpha$ lines in Fig. 1(a) including $\alpha$ decays of $^{216}$Th(7921 keV, 28 ms), $^{215}$Ac(7604, 0.17 s), $^{215}$Th(7524:7395, 1.2 s), $^{212}$Ra(6899, 13 s), $^{211}$Ra(6.910, 13 s), $^{211}$Fr(6534, 3.1 min), $^{207}$Rn(6131, 9.3 min), and $^{207}$At(5758, 1.8 h). These nuclei are produced by the reaction of the beam with $^{186}$W nucleus which is contained in the $^{198}$Pt target.

The correlation between the recoil implantation and the subsequent $\alpha$ decays were searched for within the time interval $\Delta t$(*recoil*-$\alpha$) of 10 s. We only selected chains in which the recoil implantation is followed by two or more $\alpha$ decays. We obtained 18 chains and the corresponding $\alpha$-particle energy spectrum is shown in Fig. 1(b). In this process, the condition was imposed that the recoil event generates the TOF and energy signal corresponding to the ERs on the two-dimensional spectrum to reject chance events associated with the scattered particle.

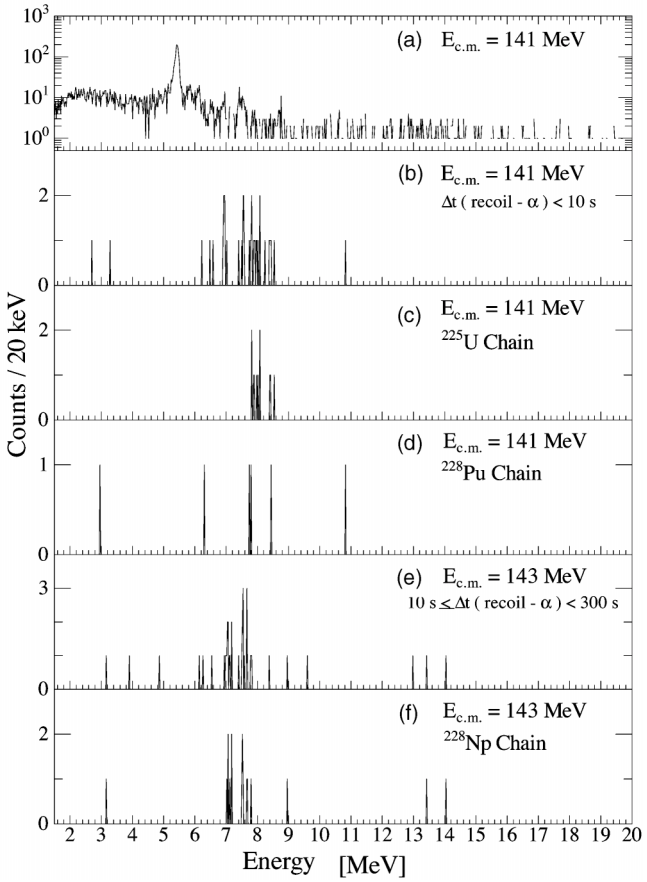


FIG. 1. Energy spectra obtained from the PSD in the reaction of $^{34}$S+$^{198}$Pt. Spectra in (a)–(d) include all data for measurements where $E_{\mathrm{c.m.}}$=141 MeV. Spectra in (e) and (f) are obtained in the measurements where $E_{\mathrm{c.m.}}$=143 MeV.

Among the 18 chains in Fig. 1(b), we found four chains starting from the $^{225}$U implantation based on detected $\alpha$-particle energies and half-lives. The $E_\alpha$ spectrum of the $^{225}$U chain is shown in Fig. 1(c). Here, the events of full energy absorption for the $\alpha$ decay of $^{225}$U itself and $^{221}$Th are selected. Table I shows the $\alpha$-decay character (kinetic energy and lifetime) for the $^{225}$U chains. When the $\alpha$-particle energy of $^{221}$Th is around 8472 keV instead of 8146 keV, the identification of the $^{225}$U chain requires the detection of $^{213}$Rn. This is because the $\alpha$-particle energies for $^{225}$U($E_\alpha$ =7879, 7821 keV)-$^{221}$Th(8472) are close to that of $^{228}$Pu(7810[1])-$^{224}$U(8466) and the lifetimes of $^{225}$U(95 ms) and $^{221}$Th(1.68 ms) are also close to that of $^{228}$Pu(1.1 s; see below) and $^{224}$U(0.9 ms), respectively. The short-lived nucleus $^{217}$Ra does not appear in Table I because of the experimental limitation. The other chains in Fig. 1(b) include those starting from $^{216}$Th (two chains) and $^{215}$Th (three chains) produced in the $^{34}$S+$^{186}$W reaction. The same process was adopted for the measurement at $E_{\mathrm{c.m.}}$ =143 MeV, in which two chains starting from the $^{225}$U implantation were found as listed in Table I.

TABLE I. $\alpha$-Decay energy (in keV) and lifetime (given in parentheses) starting from the recoil implantation of $^{225}$U ($\alpha 3n$ channel). Kinetic energy of $\alpha$ particle and half-life (in square brackets) taken from the literature [13] is shown in the first line. Intensities of $\alpha$ lines are shown in % for $^{225}$U and $^{221}$Th. The second column shows the center-of-mass energy $E_{\mathrm{c.m.}}$ in MeV.

| No. | $E_{\mathrm{c.m.}}$ (MeV) | $^{225}$U $7879^{85\%}, 7821^{15\%}$[95 ms] | $^{221}$Th $8472^{39\%}, 8146^{56\%}$[1.68 ms] | $^{217}$Ra 8992[1.6 $\mu$s] | $^{213}$Rn 8088[25 ms] |
|---|---|---|---|---|---|
| I-1 | 141 | 7828(3.2 ms) | 8415(4.6 ms) | | 8024(31 ms) |
| I-2 | 141 | 7898(47 ms) | 8071(1.7 ms) | | |
| I-3 | 141 | 7823(210 ms) | 8548(1.3 ms) | | 7976(15 ms) |
| I-4 | 141 | 7873(613 ms) | 8400(1.8 ms) | | 8074(8.1 ms) |
| I-5 | 143 | 7875(198 ms) | 8164(4.0 ms) | | |
| I-6 | 143 | 7973(99 ms) | 8238(7.2 ms) | | 8177(4.3 ms) |

The half-life of $^{225}$U was determined to be $135^{+93}_{-39}$ ms. This agrees with 80±40 ms [14] and 95±15 ms [15], where $^{225}$U is produced in the reactions of $^{180}$Hf($^{48}$Ca, $3n$) [14] and $^{209}$Bi($^{19}$F, $3n$) [15]. There are reports of a slightly shorter half-life of $30^{+20}_{-10}$ ms [16] and $59^{+5}_{-2}$ ms [17], both of which used the reaction $^{208}$Pb($^{22}$Ne, $5n$) to produce $^{225}$U.

Among the nine chains in Fig. 1(b) that were not identified in the above process, we searched for one that is followed by a long-lived nucleus with the help of position agreement. The searching time is extended to 120 min, long enough to observe the $\alpha$ decay of $^{212}$Rn ($T_{1/2}$=23.9 min [13]) as the descendant of $^{228}$Pu. In this process, we found two decay chains, and the $E_\alpha$ spectrum is shown in Fig. 1(d). They are both attributed to the $^{228}$Pu chain based on their decay character as shown in Table II. The event II-1 has the $\alpha$ decay of 10817 keV, which may be a partial pileup of $^{220}$Th and $^{216}$Ra decays. The chain is terminated by the $\alpha$ decay of $^{212}$Rn. The event II-2 is determined to be a $^{228}$Pu-chain from the decay character of $^{224}$U and the subsequent $\alpha$ decay after 11 min as the candidate for $^{212}$Rn decay. The $\alpha$ particle from $^{212}$Rn of II-2 is considered to have escaped from the PSD, and part of the energy deposition is detected in the PSD. We have estimated the probability of a chance coincidence signal of 2–20 MeV to be detected as the $\alpha$ decay in the time interval of 30 min. This depends on the counting rate of the PSD and the detection efficiency of the timing detector placed upstream the PSD. The obtained probability is 0.013. The same procedure was adopted to the $E_{\mathrm{c.m.}}$=143 MeV run. We detected two chains having decay character of $\alpha_1(E_\alpha$=7853 keV, $\tau$=4.5 ms)$-\alpha_2$(6893, 7.37 s) $-\alpha_2$(6116, 53 s) and $\alpha_1$(7617, 0.13 s)$-\alpha_2$(7048, 3.2 s) $-\alpha_3$(6316, 13 min). The former and the latter were determined to be decay chains of $^{216}$Th($E_\alpha$=7921, $T_{1/2}$=28 ms)$-^{212}$Ra(6899, 13 s)$-^{208}$Rn(6144, 24 min) and $^{214}$Th(7678, 0.1 s)$-^{210}$Ra(7019, 3.7 s)$-^{206}$Rn(6258, 5.7 min), respectively.

The half-life of $^{228}$Pu was measured to be $1.1^{+2.0}_{-0.5}$ s. Here, the error is estimated by the method in Ref. [18]. The obtained average $\alpha$-particle energy of $^{228}$Pu, 7772±35 keV, reasonably agrees with the data [1]. The present $E_\alpha$ and half-life are compared with the prediction of the Geiger-Nuttall law. In order to determine the $\alpha$-decay $Q$-value $Q_\alpha$ for $^{228}$Pu, we assumed that the detected $\alpha$ decay is from ground-state to ground-state transition, and the electron screening effect [19] is corrected for. The $Q_\alpha$(7948±36 keV) and $T_{1/2}$ are plotted in Fig. 2 together with the other data [13]. In this figure, the Geiger-Nuttall curves for elements Th, U, and Pu are drawn by using the expression and constants in Ref. [19]. Our data of $^{228}$Pu match the characteristics of Pu isotopes. This means that the $^{228}$Pu decay is dominated by the $\alpha$ decay. The dominance of $\alpha$ decay is supported by the theoretical calculation that the partial half-life for $\alpha$ decay $T_{\alpha,1/2}$=0.42 s [3] is two orders of magnitude shorter than that for EC decay $T_{\mathrm{EC},1/2}$ =44 s [4], as described in Sec. I. Even $^{230}$Pu, which has two more neutrons and so may be expected to have a larger EC branch than $^{228}$Pu, has a dominant $\alpha$-decay probability of 84% [20]. The $^{230}$Pu data shown in Fig. 2 refers to the experimental half-life of 102 s [21], $\alpha$-decay probability (84%), and $Q_\alpha$ value of 7213 keV obtained by using $E_\alpha$=7050 keV [13].

In order to find the $\alpha$ decay of $^{228}$Np with half-life of 61.4 s [6], the recoil-$\alpha$ chain was searched for in the time span of 10 s$\leqslant\Delta t(recoil-\alpha)<$300 s. We set the condition that the *recoil* implantation is followed by two or more $\alpha$ decays in this

TABLE II. $\alpha$-Decay energy (in keV) and lifetime (given in parentheses) starting from the recoil implantation of $^{228}$Pu ($4n$ channel). The literature value of kinetic energy of $\alpha$ particle and half-life (in square brackets) for $^{228}$Pu [1] and the other nuclei [13] is shown in the first line. The time with symbol "<" represents the time interval relative to the preceding $\alpha$ decay. The signal with escaped event is indicated by "*esc*." The signal of pileup, "*pil*," is caused by the $\alpha$ decays of a mother and a short-lived daughter indicated by "←."

| No. | $E_{\mathrm{c.m.}}$ (MeV) | $^{228}$Pu 7810 | $^{224}$U 8466[0.9 ms] | $^{220}$Th 8790[9.7 $\mu$s] | $^{216}$Ra 9349[0.18 $\mu$s] | $^{212}$Rn 6264[23.9 min] |
|---|---|---|---|---|---|---|
| II-1 | 141 | 7807(0.35 s) | | $10817_{pil}$(<0.77 ms) | ← | 6309(34 min) |
| II-2 | 141 | 7736(2.76 s) | 8446(3.2 ms) | | | $2960_{esc}$(11 min) |

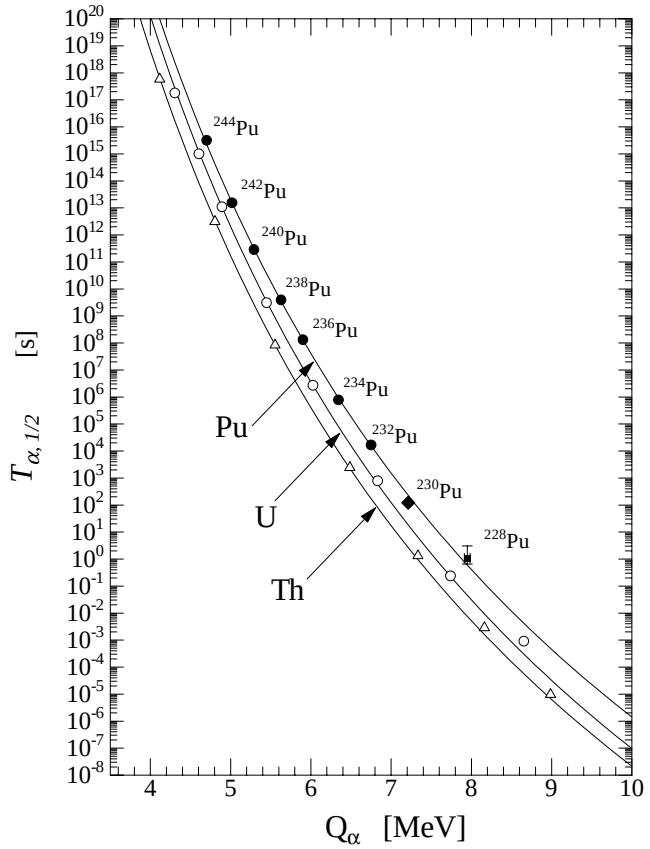


FIG. 2. $\alpha$-Decay energy and half-life for $^{228}$Pu (solid square with error bar) is plotted on the map of $T_{\alpha,1/2}$ versus $Q_\alpha$ together with the other nuclei (solid circle is for Pu, open circle for U, and open triangle for Th [13]). The $T_{\alpha,1/2}$ value for $^{230}$Pu is shown by the solid diamond. Geiger-Nuttall curve for even-even Pu, U, and Th isotopes [19] are shown by the solid curves.

time region. Figure 1(e) shows the spectrum of $E_\alpha$ for the obtained 15 decay chains in a 29-h run of $E_{\text{c.m.}}$=143 MeV. In these chains, five chains starting from $^{228}$Np are obtained as shown in the $E_\alpha$ spectrum of Fig. 1(f), and the decay properties are listed in Table III. Here, we selected events in which the full energy of an $\alpha$ decay of $^{228}$Np is absorbed. The same procedure was adopted for the $E_{\text{c.m.}}$=141 MeV measurement, but we observed no candidate for the production of $^{228}$Np.

The time interval between the recoil implantation and $^{228}$Np decay ranges from 15 s to 196 s. In finding the recoil implantation event of $^{228}$Np, the probability of a random event in 200 s is estimated to be about 17%. This probability decreases with decrease in the lifetime of the implanted ER. The obtained half-life $56^{+45}_{-17}$s of $^{228}$Np agrees with 61.4 s [6]. The daughter $^{224}$Pa has the $\alpha$-particle energy of $E_\alpha$ =7488 keV (70% abundance) and many other energies [13]. The detected four events of $^{224}$Pa are all close to the energy of the main branch. Events of III-1 and III-3 have the large energies 14048 and 13425 keV. This apparently comes from the pileup of the decays of $^{220}$Ac and $^{216}$Fr(0.7 $\mu$s). In our data acquisition system, the pulse height generated by the sequential $\alpha$ decays depends sensitively on the time interval on the sub-$\mu$ s scale, and is given by the sum of the signal of the first pulse and a portion of the second one. When the second decay is delayed by 1 $\mu$s, this signal is rejected. Thus, the reason for the large energies should be that the full energies of the $\alpha$ particles of $^{220}$Ac and $^{216}$Fr are deposited in the PSD with the time difference less than 1 $\mu$s, and part of the second signal is piled to the first one. The event III-5 does not have decay signals of $^{224}$Pa and $^{220}$Ac, but the full energy absorption of $^{216}$Fr is obtained. The time interval of this event (3.39 s) is the sum of lifetimes of $^{224}$Pa, $^{220}$Ac, and $^{216}$Fr. Astatine-212 with 0.134 s [13] has dominant ground-state to ground-state $\alpha$ decay of 7679 keV (82%) and many branches to the excited states of $^{208}$Bi. The two decays of $^{212}$At (7687 and 7658 keV) in Table III are the ground-state to ground-state transition. The 7012 keV event of III-3 seems to correspond to the 7045-keV transition which has low frequency (0.45%).

In the measurement with the beam energy $E_{\text{c.m.}}$ =143 MeV, we detected one event of a $\alpha_1$-$\alpha_2$ correlation with energies of $E_{\alpha,1}$=6679 keV and $E_{\alpha,2}$=7483 keV. The time difference between the two $\alpha$ decays was 0.49 s. They are identified to be $^{228}$U and $^{220}$Ra, respectively, in the chain [13],

$$^{228}\text{U}(E_\alpha = 6680\ \text{keV}, T_{1/2} = 9.1\ \text{min}) \rightarrow {}^{224}\text{Th}(7170, 1.05\ \text{s}) \rightarrow {}^{220}\text{Ra}(7455, 18\ \text{ms}) \rightarrow {}^{216}\text{Rn}(8050, 45\ \mu\text{s}) \rightarrow {}^{212}\text{Po}(8784, 0.3\ \mu\text{s}) \rightarrow {}^{208}\text{Pb}.$$

Since the $\alpha$ particle from $^{224}$Th escaped from detection by

TABLE III. $\alpha$-Decay energy (in keV) and lifetime starting from the recoil implantation of $^{228}$Np ($p3n$ channel). The literature value for $^{228}$Np [6] and the other nuclei [13] is shown in the first line. See the captions of Tables I and II for the detailed explanation.

| No. | $E_{\text{c.m.}}$ | $^{228}$Np | $^{224}$Pa | $^{220}$Ac | $^{216}$Fr | $^{212}$At |
|---|---|---|---|---|---|---|
| | | [61.4 s] | $7488^{70\%}$[0.79 s] | $7855^{26\%}$[26.4 ms] | 9005[0.7 $\mu$s] | $7679^{82\%}$, $7045^{0.45\%}$[0.314 s] |
| III-1 | 143 | 7183(29 s) | 7529(1.10 s) | $14048_{pil}$(3.7 ms) | ← | $3170_{esc}$(0.070 s) |
| III-2 | 143 | 7062(128 s) | 7543(0.20 s) | 7794(58 ms) | | 7687(2.4 ms) |
| III-3 | 143 | 7126(196 s) | 7495(0.56 s) | $13425_{pil}$(21 ms) | ← | 7012(0.12 s) |
| III-4 | 143 | 7177(35 s) | 7521(3.03 s) | | | 7658(0.18 s) |
| III-5 | 143 | 7065(15 s) | | | 8969(<3.39 s) | |

the PSD, the measured time interval 0.49 s is the sum of lifetimes of $^{224}$Th and $^{220}$Ra. Radon-216 and $^{212}$Po were not detected due to the dead time of our data acquisition system. The implantation event to the PSD was found at 18 min before the $\alpha$ decay of $^{228}$U. Because of the increased probability of a random event in such a long time span in searching for the recoil implantation event, we can only state that 18 min is the lower limit for the lifetime of $^{228}$U. The $^{228}$U is not directly produced as an ER in the present reaction but is produced as a daughter of the EC decay of $^{228}$Np. The detected number of $\alpha$-decay events for $^{228}$U (one event) and $^{228}$Np (five events) leads to the $\alpha$-decay probability of $83^{+17}_{-36}$% for $^{228}$Np. This is comparable to $40^{+8}_{-6}$% reported by Kreek *et al.* [6], which they determined by measuring the $^{216}$Fr(9005 keV, 0.7 $\mu$s) and $^{212}$Po, which are the descendants of the $\alpha$-decay chains starting from $^{228}$Np and $^{228}$U.

From the mass table of Audi and Wapstra [22], the $\alpha$-decay $Q$-value $Q_\alpha$ of $^{228}$Np is obtained to be 7415 keV. This results in the $\alpha$-decay energy of 7285 keV for the ground-state to ground-state $\alpha$ decay of $^{228}$Np. This is 100–220 keV larger than the experimental data. A possible reason is that the $\alpha$ decay predominantly produces the excited states of $^{224}$Pa.

We determined the ER cross sections for $^{228}$Pu, $^{228}$Np, and $^{225}$U. The results are shown in Fig. 3. The errors are in the margin of the statistical error. The data were compared to a statistical model calculation. For this purpose, the partial wave cross section for the fusion $^{34}$S+$^{198}$Pt was calculated by using the CCDEF code [23], which was then inputted to the HIVAP code [24] to calculate the surviving probability and the ER cross section of the specific channel. In the CCDEF code, we took into account the couplings to inelastic channels of the projectile and target. For $^{34}$S, deformation parameter (excitation energy) of the quadrupole and octupole vibrations are $\beta_2$=0.252 (2.13 MeV) [25] and $\beta_3$=0.330 (4.62 MeV) [26], respectively. $\beta_3$=0.05 (1.68 MeV) [26] was adopted for the octupole vibration of $^{198}$Pt. We also took into account the static deformation of $^{198}$Pt ($\beta_2$=−0.060 [27], $\beta_4$=−0.030 [28]). The calculated fusion cross section $\sigma_{\rm fus}$ is shown on the upper section of Fig. 3 by the dashed curve. The dotted curve is the result of the one-dimensional barrier penetration model, which gives the barrier height of 141.1 MeV. The ER cross sections calculated by the HIVAP code are shown by the solid curve in each section of the figure. We have to adjust the factor $b_{\rm fac}$, by which the fission barrier height of the liquid-drop part [29] is multiplied to calculate the fission barrier $B_{\rm f}=b_{\rm fac}B_{\rm LDM}-\delta W$ from 1.03 [12] to 1.00 so as to obtain reasonable agreement with the experimental data. The $\delta W$ is the ground-state shell energy correction. The change of the factor reduces the $B_{\rm f}$ value by the amount of 0.11 MeV for $^{232}$Pu. This modification reduces the cross section by a factor of about 2 with the beam energy which yields the highest cross section for each channel being unchanged.

The experimental ER cross section $17^{+2.2}_{-1.3}$ nb of the 4$n$ channel at $E_{\rm c.m.}$=141 MeV in the fusion reaction $^{34}$S+$^{198}$Pt was close to 4±2 nb of the 4$n$ channel of $^{24}$Mg+$^{208}$Pb reaction at $E_{\rm c.m.}$=118 MeV [1] which forms the same compound nucleus $^{232}$Pu. For the $^{24}$Mg+$^{208}$Pb reaction, we also calculated the cross sections of $^{228}$Pu with the same procedure. In the CCDEF calculation, we used deformation parameters $\beta_2$ =0.606 (1.37 MeV) [25] and $\beta_3$=0.250 (7.62 MeV) [26] to take into account the couplings to the excited states of $^{24}$Mg. For the excitation of $^{208}$Pb, parameters $\beta_2$ =0.054 (4.09 MeV) [25] and $\beta_3$=0.110 (2.61 MeV) [26] are adopted. The calculated result is 6 nb at $E_{\rm c.m.}$=118 MeV, reproducing the experimental data in Ref. [1]. Since the excitation energy, $E_{\rm ex}$=43 MeV, of $^{34}$S+$^{198}$Pt at $E_{\rm c.m.}$=141 MeV is close to $E_{\rm ex}$=44 MeV of $^{24}$Mg+$^{208}$Pb at $E_{\rm c.m.}$=118 MeV, the survival probabilities for both systems are nearly identical. The fusion cross section given by the CCDEF code is $\sigma_{\rm fus}$=69 mb of $^{34}$S+$^{198}$Pt, which agrees with $\sigma_{\rm fus}$=184 mb of $^{24}$Mg+$^{208}$Pb within factor of ~3.

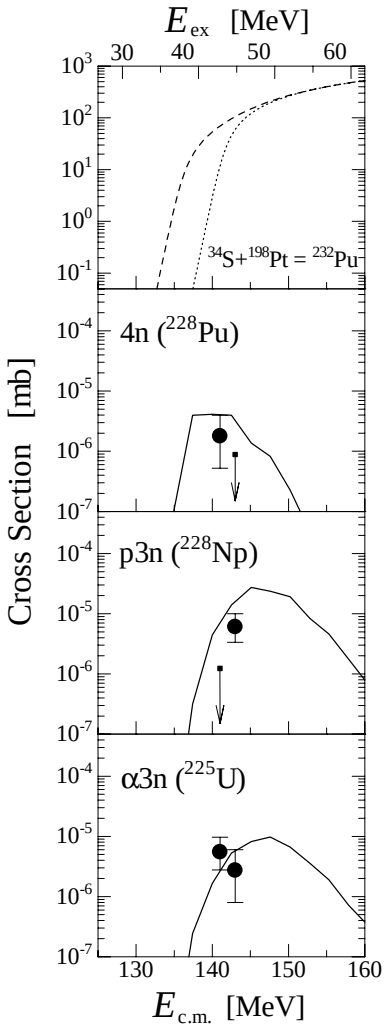


FIG. 3. Evaporation residue cross sections for $^{228}$Pu, $^{228}$Np, and $^{225}$U are shown together with the statistical model calculation (solid curve). The vertical bar with arrow shows the upper limit of the cross section. The fusion cross section calculated by the CCDEF code is shown by the dashed curve, and the fusion cross section of the one-dimensional barrier penetration model is shown by the dotted curve.

## IV. SUMMARY

The fusion reaction $^{34}S+^{198}Pt$ was used to produce $^{228}Pu$ as the evaporation residue and its half-life was measured to be $1.1^{+2.0}_{-0.5}$ s for the first time. The present half-life follows the Geiger-Nuttall curve for even-even Pu isotopes, which shows that $\alpha$ decay is the dominant decay mode. In this reaction, five $\alpha$ decays of $^{228}Np$ were observed for the first time. The ER cross sections of $^{228}Pu(4n)$, $^{228}Np(p3n)$, and $^{225}U(\alpha 3n)$ were reproduced by a statistical model calculation.

## ACKNOWLEDGMENTS

The authors thank the crew of the JAERI-tandem facility for the beam operation. Thanks are due to Dr. T. Ishii and I. Nishinaka of JAERI for fruitful discussions with them. One of us (C.J.L.) acknowledges the Japan Society for the Promotion of Science (JSPS), Grant No. PB01003.

[1] A. N. Andreyev, D. D. Bogdanov, V. I. Chepigin, A. P. Kabachenko, O. N. Malyshev, A. G. Popeko, R. N. Sagaidak, G. M. Ter-Akopian, M. Veselsky, and A. V. Yeremin, Z. Phys. A **347**, 225 (1994).

[2] H. Ikezoe, Y. Nagame, T. Ikuta, S. Hamada, I. Nishinaka, and T. Ohtsuki, Nucl. Instrum. Methods Phys. Res. A **376**, 420 (1996).

[3] H. Koura, J. Nucl. Radiochem. Sci. **3**, 201 (2002).

[4] T. Tachibana and M. Yamada, in *Proceedings of the Inc. Conference on Exotic Nuclei and Atomic Masses, Arles, 1995*, edited by M. de Saint and O. Sorlin (Editions Frontieres, Gif-sur-Yvette, 1995), p. 763.

[5] V. I. Kuznetsov, N. K. Skobelev, and G. N. Flerov, Sov. J. Nucl. Phys. **4**, 202 (1967).

[6] S. A. Kreek, H. L. Hall, K. E. Gregorich, R. A. Henderson, J. D. Leyba, K. R. Czerwinski, B. Kadkhodayan, M. P. Neu, C. D. Kacher, T. M. Hamilton, M. R. Lane, E. R. Sylwester, A. Türler, D. M. Lee, M. J. Nurmia, and D. C. Hoffman, Phys. Rev. C **50**, 2288 (1994).

[7] T. Kuzumaki, H. Ikezoe, S. Mitsuoka, T. Ikuta, S. Hamada, Y. Nagame, I. Nishinaka, and O. Hashimoto, Nucl. Instrum. Methods Phys. Res. A **437**, 107 (1999).

[8] H. Wollnik, J. Brezina, and M. Berz, Nucl. Instrum. Methods Phys. Res. A **258**, 408 (1987).

[9] A. Gavron, Phys. Rev. C **21**, 230 (1980).

[10] J. F. Ziegler, J. P. Biersack, and U. Littmark, *The Stopping and Range of Ions in Solids* (Pergamon, New York, 1985).

[11] K. Shima, T. Ishihara, and T. Mikuno, Nucl. Instrum. Methods Phys. Res. **200**, 605 (1982).

[12] S. Mitsuoka, H. Ikezoe, K. Nishio, and J. Lu, Phys. Rev. C **62**, 054603 (2000); K. Nishio, H. Ikezoe, S. Mitsuoka, and J. Lu, Phys. Rev. C, **62**, 014602 (2000).

[13] R. B. Firestone, in *Table of Isotopes*, edited by V. S. Shirley (Wiley, New York, 1996).

[14] F. P. Heßberger, H. Gäggeler, P. Armbruster, W. Brüchle, H. Folger, S. Hofmann, D. Jost, J. V. Kratz, M. E. Leino, G. Münzenberg, V. Ninov, M. Schädel, U. Scherer, K. Sümmerer, A. Türler, and D. Ackermann, Z. Phys. A **333**, 111 (1989).

[15] K. S. Toth, H. J. Kim, J. W. McConnell, C. R. Bingham, and D. C. Sousa, Phys. Rev. C **45**, 856 (1992).

[16] A. N. Andreev, D. D. Bogdanov, A. V. Eremin, A. P. Kabachenko, O. A. Orlova, G. M. Ter-Akop'yan, and V. I. Chepigin, Sov. J. Nucl. Phys. **50**, 381 (1989).

[17] F. P. Heßberger, S. Hofmann, D. Ackermann, V. Ninov, M. Leino, S. Saro, A. Andreyev, A. Lavrentev, A. G. Popeko, and A. V. Yeremin, Eur. Phys. J. A **8**, 521 (2000).

[18] K.-H. Schmidt, C.-C. Sahm, K. Pielenz, and H.-G. Clerc, Z. Phys. A **316**, 19 (1984).

[19] J. O. Rasmussen, *Alpha, Beta, and Gamma-ray Spectroscopy* (North-Holland, Amsterdam, 1966), Vol. 1, p. 701.

[20] P. T. Greenlees, P. Kuusiniemi, N. Amzal, A. Andreyev, P. A. Butler, K. J. Cann, J. F. C. Cocks, O. Dorvaux, T. Enqvist, P. Fallon, B. Gall, M. Guttormsen, D. Hawcroft, K. Helariutta, F. P. Hessberger, F. Hoellinger, G. D. Jones, P. Jones, R. Julin, S. Juutinen, H. Kankaanpää, H. Kettunen, M. Leino, S. Messelt, M. Muikku, S. Ødegard, R. D. Page, A. Savelius, A. Schiller, S. Siem, W. H. Trzaska, T. Tveter, and J. Uusitalo, Eur. Phys. J. A **6**, 269 (1999).

[21] P. Cagarda, S. Antalic, D. Ackermann, F. P. Heßberger, S. Hofmann, B. Kindler, J. Kojouharova, B. Lommel, R. Mann, A. G. Popeko, Š. Šáro, J. Uusitalo, and A. V. Yeremin, GSI report, 2002.

[22] G. Audi and A. H. Wapstra, Nucl. Phys. **A595**, 409 (1995).

[23] J. O. Fernández Niello, C. H. Dasso, and S. Landowne, Comput. Phys. Commun. **54**, 409 (1989).

[24] W. Reisdorf and M. Schädel, Z. Phys. A **343**, 47 (1992).

[25] S. Raman, C. H. Malarkey, W. T. Milner, C. W. Nestor, Jr., and P. H. Stelson, At. Data Nucl. Data Tables **36**, 1 (1987).

[26] R. H. Spear, At. Data Nucl. Data Tables **42**, 55 (1989).

[27] P. Raghavan, At. Data Nucl. Data Tables **42**, 189 (1989).

[28] P. Möller, J. R. Nix, W. D. Myers, and W. J. Swiatecki, At. Data Nucl. Data Tables **59**, 185 (1995).

[29] S. Cohen, F. Plasil, and W. J. Swiatecki, Ann. Phys. (N.Y.) (N.Y.) **82**, 557 (1974).